High Power Laser Science and Engineering, (2024), Vol. 12, e29, 8 pages.
doi:10.1017/hpl.2024.8

HIGH POWER LASER SCIENCE AND ENGINEERING

RESEARCH ARTICLE

Brightness enhancement on random-distributed-feedback Raman fiber lasers pumped by multimode diodes

Xiulu Hao[1], Chenchen Fan[1], Yang Li[1], Zhiyong Pan[1,2], Jinyong Leng[1,2], Tianfu Yao[1,2], Bing Lei[1], and Pu Zhou[1]

[1] *College of Advanced Interdisciplinary Studies, National University of Defense Technology, Changsha, China*

[2] *Nanhu Laser Laboratory, National University of Defense Technology, Changsha, China*

(Received 22 November 2023; revised 5 January 2024; accepted 6 February 2024)

Abstract

The power scaling on short wavelength (SW) fiber lasers operating around 1 μm are in significant demand for applications in energy, environment and industry. The challenge for performance scalability of high-power SW lasers based on rare-earth-doped fiber primarily lies in the physical limitations, including reabsorption, amplified spontaneous emission and parasitic laser oscillation. Here, we demonstrate an all-fiberized, purely passive SW (1018 nm) random-distributed-feedback Raman fiber laser (RRFL) to validate the capability of achieving high-power output at SWs based on multimode laser diodes (LDs) direct pumping. Directly pumped by multimode LDs, the high-brightness RRFL delivers over 656 W, with an electro-optical efficiency of 20% relative to the power. The slope efficiency is 94%. The beam quality M^2 factor is 2.9 (which is ~20 times that of the pump) at the maximum output signal power, achieving the highest brightness enhancement of 14.9 in RRFLs. To the best of our knowledge, this achievement also represents the highest power record of RRFLs utilizing multimode diodes for direct pumping. This work may not only provide a new insight into the realization of high-power, high-brightness RRFLs but also is a promising contender in the power scaling of SWs below 1 μm.

Keywords: fiber laser; purely passive gain; random distributed feedback; stimulated Raman scattering

1. Introduction

High-power short wavelength (SW) fiber lasers operating around 1 μm with high-brightness are highly required in many applications, such as material processing, nonlinear frequency conversion, spectral beam combining, etc.[1–4]. Meanwhile, due to the lower fractional thermal load as a result of the higher quantum efficiency, the thresholds of the transverse mode instability (TMI)[5–7] for SW fiber lasers based on ytterbium-doped fiber lasers (YDFLs) are usually higher than those for longer-wavelength fiber lasers operating around 1080 nm, which makes SW fiber lasers promising for high-power systems[8,9]. However, due to the significantly higher levels of amplified spontaneous emission (ASE) induced by large signal absorption cross-sections[10], high-power fiber laser systems operating at SWs around or below 1 μm[11] are found to be much more challenging compared to traditional wavelength band fiber lasers[12].

At present, most of SW output schemes are based on solid-state lasers, such as laser diodes (LDs)[13]. One of the interesting possibilities is to directly pump purely passive fibers using the available high-power multimode LDs at 915–950 nm. This approach facilitates the generation of high-power Raman lasing within the wavelength range of 960–1020 nm, presenting a set of challenges for rare-earth (RE)-doped fiber lasers[14]. A commonly utilized special wavelength in YDFLs is 1018 nm, which is located near the 1 μm band. Notably, this wavelength holds importance for tandem pumping of YDFLs, as discussed in Refs. [15–18]. Studies of this wavelength range can establish a robust experimental foundation for achieving higher power outputs in even shorter wavelength bands.

Currently, high-power 1018 nm fiber lasers are primarily realized utilizing two main structures: amplifier-based[14–17] and oscillator-based configurations[18–25]. In the case of the 1018 nm all-fiber master oscillator power amplifier (MOPA), studies in this area have been limited due to the issue of reabsorption in the 1018 nm wavelength range[15]. As a result, there have been limited reported achievements, with output powers reaching around 616 W[17]. Compared to amplifiers, 1018 nm oscillators have a simpler and more stable structure.

Correspondence to: Tianfu Yao and Pu Zhou, College of Advanced Interdisciplinary Studies, National University of Defense Technology, Changsha 410073, China. Email: yaotianfumary@163.com (T. Yao); zhoupu203@163.com (P. Zhou)

While these studies show the potential of high-power oscillators, it is worth noting that the presence of resonator cavity structures in oscillators can lead to the occurrence of self-pulsing phenomena[26,27]. This phenomenon leads to the occurrence of nonlinear effects, such as stimulated Raman scattering (SRS), in high-power fiber laser systems[28,29]. Furthermore, the traditional structure based on the RE-doped fiber oscillator is no longer suitable for SW output, making it incapable of achieving higher laser output power. Therefore, it is crucial to explore new and innovative approaches for the development of SW lasers.

As a novel fiber light source, random-distributed-feedback Raman fiber lasers (RRFLs) have attracted widespread attention due to their unique performance since they were initially introduced by Turitsyn *et al.*[30] in 2010 and further explored by Ye *et al.*[31,32]. In the past, limited by the brightness of LDs, researchers could only employ YDFLs pumped by LDs to pump RRFLs, thereby achieving higher output power. However, the two-stage conversion for signal light through pumping results in low electro-optical (EO) efficiency (less than 20%) of the laser system[13]. With the development of high-brightness LDs and high-nonlinear fiber technology, obtaining laser output based on direct pumping of passive fibers by LDs will be a new technological solution for achieving SW lasers in the future[33–36]. In 2018, Evmenova *et al.*[33] demonstrated the first random lasing in the all-fiber scheme of direct pumping by LDs, with output power of 27 W and beam quality M^2 of 1.6 at 996 nm. Although further power scaling is constrained by relatively poor pump brightness, the novel routine on wavelength expanding beyond the general band of YDFLs has been validated[34–37]. Therefore, RRFLs pumped by multimode diodes are attractive to achieve higher power lasers at SWs[34]. The combination of high-brightness multimode LDs and purely passive fibers will yield a notable 'performance doubling' effect in generating SWs.

In this paper, we firstly demonstrate a half-open cavity all-fiberized SW (1018 nm) RRFL directly pumped by multimode diodes, excluding any RE-dopant in the whole system. The potential on power scaling of SW RRFLs directly pumped by multimode LDs has been verified by the obtained output power of 656 W. The slope efficiency is 94% and the EO conversion efficiency is approximately 20%. To the best of our knowledge, this result also represents the highest power record of RRFLs utilizing multimode LDs for direct pumping with SW output, showing great potential at power scaling at SWs below 1 μm. We achieve a signal light output M^2 of 2.9 (which is ~20 times that of the pump), resulting in a brightness enhancement (BE) of 14.9, the highest known BE in RRFLs to date. The findings and techniques explored in this study could pave the way for achieving high-power SW laser output through multimode LD direct pumping of passive fibers, providing a new insight into the realization of high-power, high-brightness RRFLs below 1 μm.

2. Experimental setup

The experimental setup for the purely passive RRFLs pumped by multimode LDs is depicted in Figure 1. Accordingly, the laser system in Figure 1(a) follows a simple half-open cavity configuration and the LD directly-pumped RRFLs significantly enhance system integration. The output of the pump system (as depicted in the illustration) is provided by a multimode diode module with adjacent wavelengths, ranging from 954 to 986 nm, totaling 13 LDs with approximately 3 nm wavelength spacing. The laser from these LDs is coupled into the core of a commercial fiber using a volume Bragg grating (VBG). The core and cladding diameters of this fiber are 100 and 360 μm, respectively, with a core numerical aperture (NA) of 0.22. The maximum output power of the coupled pump is measured to reach 1915 W with a coupling efficiency of 98%. The brightness[38,39] of the output multi-wavelength pump after spectral synthesis is about 6.7×10^{16} W/(m^2·sr). The output spectrum of the pump is measured at maximum output, as depicted in Figure 1(b).

The combined pump radiation is directed into a section of passive fiber with a 100/140 μm core/cladding diameter and a fiber core NA of 0.25. After comparing the results obtained with various fiber lengths, it was concluded that an optimal fiber length of approximately 220 m should be used. Further power scaling and conversion efficiency are limited by the power and brightness of the LDs. Subsequently, it is introduced into a half-open cavity where a 1018 nm high-reflectivity fiber Bragg grating (HR FBG) and RDFB (random distributed feedback) within a section of commercial purely passive multimode graded-index (GRIN) fiber are present. The HR FBG, with a reflectivity exceeding 99% at a center wavelength of 1017.7 nm, exhibits a relatively narrow linewidth of 1.97 nm at 3 dB linewidth. The reflection spectrum of the HR FBG is shown in Figure 1(a). The FBG with the mode-selection properties is ultraviolet (UV)-inscribed and has the same diameter and fiber core NA as the passive 100/140 μm multimode GRIN fiber used. The transmission loss of the GRIN fiber is 1.5 dB/km at 976 nm. The output pigtailed fiber of the half-open cavity is spliced to a matched end cap (EC), which could avoid the damage to the fiber end face. To characterize the output radiation, the collimated beam is split into the individual pump and signal beams by dichroic mirrors (reflectivity > 99%@1018 nm; transmissivity > 99%@954–986 nm), whose power, spectrum and beam quality parameters are measured respectively. For the signal laser, after filtering out the residual pump, the beam profiles and beam quality are examined using a charge-coupled device (CCD) camera and a beam quality monitor. In addition, an oscilloscope is employed to capture the time-domain intensity data of the output beam. The output signal spectrum of the RRFLs is illustrated in Figure 1(d).

https://doi.org/10.1017/hpl.2024.8 Published online by Cambridge University Press

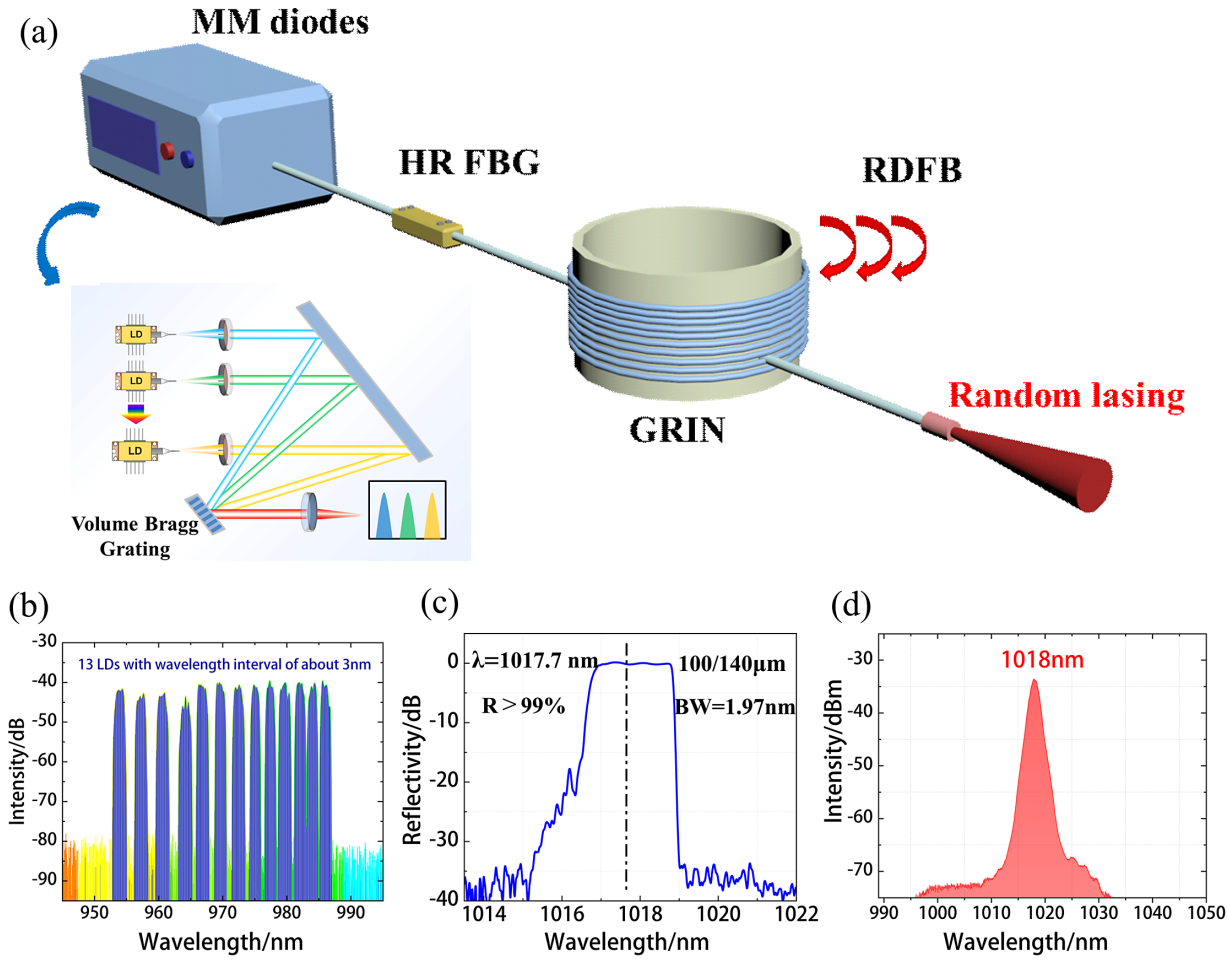

Figure 1. Random-distributed-feedback Raman fiber laser experimental setup. (a) Simplified RRFLs with LD direct pumping. (b) The output spectrum of the pump. (c) The reflection spectrum of the HR FBG. (d) The output spectrum of signal light. MM-LDs, multimode laser diodes; HR FBG, high-reflection fiber Bragg grating; GRIN, graded index; RDFB, random distributed feedback.

3. Results and discussion

Building upon this experimental configuration, we conducted an in-depth investigation of the output characteristics of an SW (1018 nm) RRFL in the frequency, spatial and temporal domains. This study aimed to gain a comprehensive understanding of its spatiotemporal dynamics, thereby providing a solid experimental foundation for future shorter wavelength system design[40,41].

3.1. Output characteristics of the SW (1018 nm) RRFL

Firstly, we analyzed and discussed the frequency spectrum output characteristics of the 1018 nm RRFLs as a function of the signal light power. Figure 2 illustrates the influence of input pump power on the output signal characteristics. In Figure 2(a), the power spectrum of the filtered RRFLs is depicted at different output powers. At a signal power of only 10 W, higher-order Stokes light emerges at 1070 and 1123 nm. These wavelengths correspond to second-order and third-order Raman shifts, respectively, and are close to the Raman gain peak of the silica-based fiber at around 13.2 THz. As the signal power increases to 276 W, the intensity of the higher-order Stokes light at these wavelengths weakens significantly. When the signal light power exceeds 276 W, the higher-order Stokes light disappears. The observed changes in the spectral characteristics are closely related to the distinctive half-open cavity structure of the random laser[32,42,43].

The cause of this behavior can be attributed to the process of cascaded stimulated Brillouin scattering (SBS)[32]. In cavity-free random fiber lasers, incident photons propagating through a long passive fiber can be backscattered by the random refractive index and inhomogeneity-induced weak Rayleigh scattering, and amplified by SRS. At the same time, the acoustic field generated by electrostriction induces moving, random density gratings, a process defined as SBS[42,43]. Then, photons experiencing a frequency downshift due to the Doppler effect are excited by the transient temporal characteristics. The three insets with output power from 10 to 276 W at the bottom present the output spectrum near the threshold, while the other three insets at the top

https://doi.org/10.1017/hpl.2024.8 Published online by Cambridge University Press

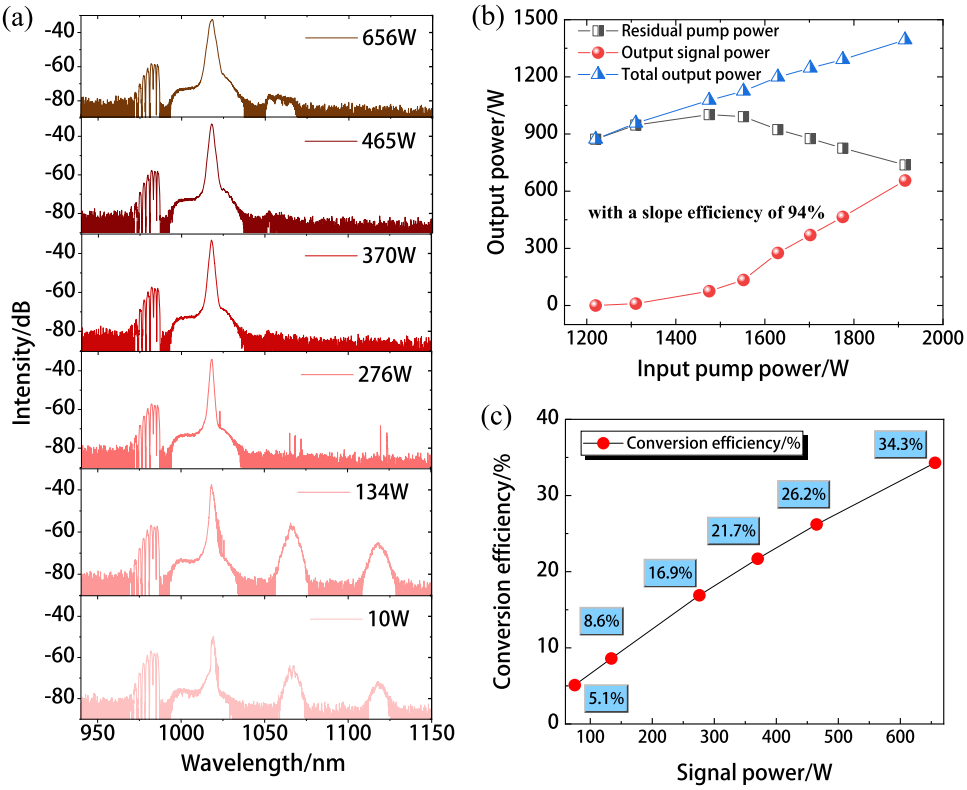

Figure 2. Output signal spectrum and power of RRFLs. (a) Output spectrum at different signal optical power levels. (b) Evolution characteristics of signal light power with injected pump light power. (c) The optical-to-optical conversion efficiency of signal light.

present the output spectrum well above the threshold. In the following section, we delve into a more detailed analysis by considering its temporal characteristics. To characterize the output radiation, the collimated beam is split into the individual pump and signal beams by the dichroic mirrors. With the increase in wavelength, the corresponding transmissivity also decreases, resulting in the residual pump being more than 975 nm, more than 20 dB higher than the residual pump at 955–965 nm.

To gain a more visually intuitive understanding of the pump–signal light conversion relationship, a schematic diagram is presented in Figure 2(b). It can be observed that when the injected pump power reaches 1310 W, the signal light begins to be emitted. Due to the half-open cavity structure of the random fiber laser, the weak RDFB inside the fiber provides backward feedback, resulting in a higher emission threshold for the signal light compared to an oscillator. As the pump power exceeds 1310 W, the power of the signal laser at 1018 nm experiences a rapid increase. With further augmentation of the injected pump power, the pump energy swiftly converts into signal light. At the maximum pump power of 1915 W, the signal power reaches 656 W, yielding a corresponding slope efficiency of 94%. The further increase in power is limited by the combined effects of higher-order Raman and pump conversion efficiency. The suppression of higher-order Raman scattering can be achieved by shortening the length of the fiber; however, this leads to an undesirable consequence of more residual pump light, significantly decreasing the pump's conversion efficiency. Hence, by balancing both higher-order Raman scattering and pump conversion efficiencies, we achieved an output power of 656 W.

The optical-to-optical (O-O) conversion efficiency of the laser system is the ratio of the signal light power to the input pump light power, while the EO efficiency includes the power from the power supply to the fiber laser. The O-O conversion efficiency of the signal light is depicted in Figure 2(c). Through computation, it is revealed that as the injected pump power increases, the conversion efficiency of the signal light steadily improves, reaching a remarkable efficiency of 34.3% at the highest power level. Although there is too much residual pump power in the final output beam (more than 50%) and the total O-O conversion efficiency for this system is only 34.3%, the EO efficiency of this system can reach 20%[12]. This efficiency is comparable to that of a two-stage conversion (from LDs to YDFLs, and then from YDFLs to RRFLs).

Furthermore, we conducted an analysis of the changes in signal light linewidth as the signal power increases. In Figure 3, a distinct 'notch' pattern can be observed in the signal light linewidth. Specifically, as the signal power increases, the linewidth initially decreases and then starts to increase.

https://doi.org/10.1017/hpl.2024.8 Published online by Cambridge University Press

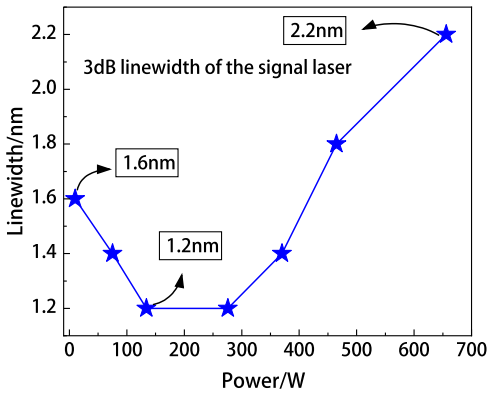

Figure 3. The output 3 dB linewidth of the signal laser at different output power levels.

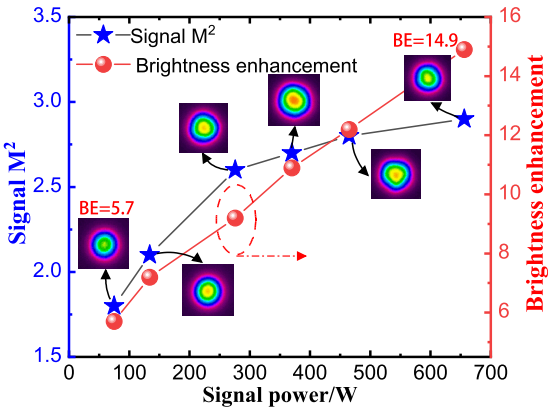

Figure 4. Beam quality factor M^2 (left-hand axis) and the corresponding brightness enhancement (right-hand axis) at different signal light power levels.

At an output power of 10 W, the signal light linewidth measures at 1.6 nm, and the minimum linewidth of around 1.2 nm is achieved at a power of approximately 200 W (this process corresponds to the gradual stabilization of the random fiber laser in the frequency domain, as depicted in Figure 2(a)). After the frequency domain stabilization of the random fiber laser, the signal light linewidth gradually increases with power, reaching a linewidth of 2.2 nm at the highest power level.

Owing to the typical Schawlow–Townes spectral narrowing effect and the cascaded SBS effect of RDFB fiber lasers near the lasing threshold[43], the RRFL pumped by LDs shows a relatively broad spectrum near the threshold. As the pump power increases, the cascaded SBS effect gradually diminishes, leading to the stabilization of the RRFL output temporal characteristics, resulting in a more stable output spectrum and a narrower linewidth of 1.2 nm. Once the output temporal characteristics of the RRFL reach stability, with the continued increase in power from 280 to 656 W, the influence of effects such as dispersion and mode coupling within the GRIN fiber causes a further broadening of the linewidth of the signal light. In Ref. [32], the spectral evolution characteristics of the RRFL, based on temporally stable ASE pump sources, also exhibit a phenomenon of initially narrowing and subsequently broadening.

3.2. Spatial domain characteristics of the SW (1018 nm) RRFL

Secondly, we conducted an investigation into the spatial characteristics of the RRFLs. Figure 4 illustrates the remarkable improvement in beam quality of the output signal light compared to the LD pump source, with a beam quality factor of approximately 20. The left-hand axis depicts the beam quality of signal light at different power levels, while the right-hand axis shows the corresponding BE. At a signal power of around 100 W, the beam quality measures at a commendable factor of 1.8. Although there is a slight degradation in beam quality with increasing power, reaching a factor of 2.9 at the highest output power, the BE continues to exhibit linear growth. At the peak power, the brightness is enhanced by a factor of 14.9. This is currently the highest known BE in RRFL structures. In Figure 4, we can also notice that, despite the continuous increase in brightness, the beam quality of the signal light is gradually deteriorating. This is primarily attributed to the rapid conversion of pump to Stokes light within the fiber core, leading to the accumulation of heat[44]. Consequently, this heat accumulation gives rise to the thermal lens effect generated in the fiber core. Reference [44] investigated the thermal dissipation of a Raman fiber laser utilizing a purely passive fiber as the gain medium. Through simulations of power distribution, the thermal characteristics of the Raman fiber laser, including the transverse and longitudinal distributions of heat load density, temperature and thermally induced refractive index changes in the fiber, were analyzed.

To further investigate the spatial characteristics of the pump light and the resulting Stokes signal laser in the RRFLs, we conducted measurements of the beam quality factors for both the pump light and the signal light, analyzing their evolution with respect to power. Figure 5 displays the measured data for the beam quality factors of the pump and the signal light at maximum power. A clear comparison reveals that the pump light's beam profile (as shown in Figure 5(a)) exhibits a speckle pattern, while the signal light's beam profile (as shown in Figure 5(b)) at the highest power level displays a Gaussian distribution. The insets within Figure 5 provide a visual representation of the near-field beam profile. The mechanisms underlying the BE have been extensively documented in various publications[45,46]. Although the ability of GRIN fiber for power scaling and BE has been proved in an amplifier structure[47], the brightness of seed light plays a crucial role in the amplifier. In our work, the RRFL does not have seed light or a low-reflection grating with mode-selecting effects. Therefore, compared to

https://doi.org/10.1017/hpl.2024.8 Published online by Cambridge University Press

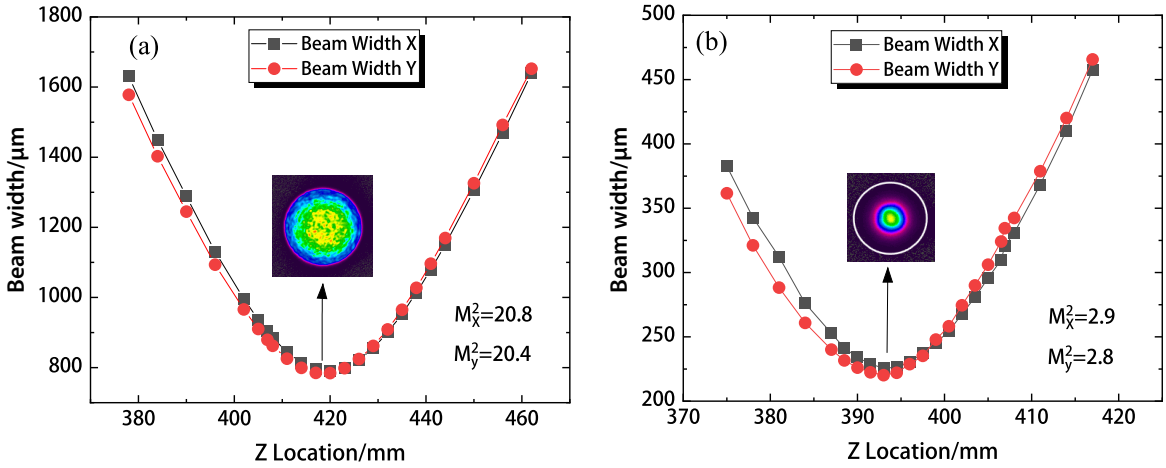

Figure 5. (a) Beam quality of pump light and (b) beam quality of signal light at maximum power.

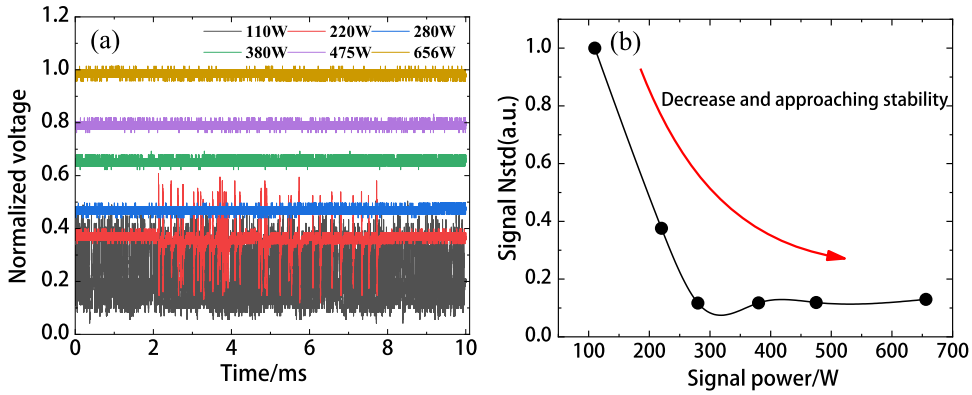

Figure 6. (a) The temporal stability characteristics of the RRFL output signal light. (a) The normalized time-domain measurement result of the RRFL signal output at various power levels. (b) The normalized standard deviation (NSTD) of the output signal light intensity.

previous work[13], this work is not only structurally innovative but also further verifies the brightness improvement and power scaling capabilities based on GRIN fibers.

Moreover, the utilization of GRIN fiber in random fiber lasers directly pumped by multimode LDs plays a vital role in enhancing the brightness. Due to the lower brightness of multimode LDs compared to YDFLs, there are more higher-order modes present, leading to a more complex coupling process between different modes. By leveraging the Raman clean-up effect within GRIN fiber, unwanted higher-order modes can be effectively suppressed, resulting in improved beam quality[48]. In conclusion, the SW (1018 nm) RRFL, which is pumped directly by LDs, demonstrates significant enhancement in the beam quality of the signal light, making it an ideal pump brightness converter in SW output[49].

3.3. Temporal domain characteristics of the SW (1018 nm) RRFL

Thirdly, the temporal characteristics of the RRFL, which directly influence the observed unique spectral changes, are analyzed. Figure 6(a) displays the normalized time-domain measurement results of the RRFL signal output at different power levels over a 10 ms time scale, utilizing an oscilloscope with a 1 GHz bandwidth. Since random fiber lasers lack a well-defined resonant cavity structure, their optical cavity dynamics are more intricate. During the initial stages of operation, the temporal stability of the random fiber laser experiences significant fluctuations. This phenomenon can also account for the presence of higher-order Raman peaks at 1070 and 1120 nm, as shown in Figure 2(a), even with a mere 10 W of signal light power. The initial temporal instability results in the generation of intense pulse signals, facilitating the manifestation of higher-order SRS effects.

Due to the influence of cascaded SBS effects, the SBS factor can switch the quality factor (Q-value) of the RRFL and is present during the power escalation process[43]. Owing to the inherent stochastic nature of the SBS effect, unstable self-pulses with random intervals, durations and amplitudes are observed. Furthermore, due to the impact of the SBS effect, the majority of pulses have such weak intensities that they are nearly submerged beneath the noise baseline. The first purely passive SW RFL directly pumped by multimode

https://doi.org/10.1017/hpl.2024.8 Published online by Cambridge University Press

LDs was reported in Ref. [50], where the observation of unstable pulses with higher Stokes orders at a 1 W power level was also reported for the first time.

After the signal light power surpasses 280 W, the temporal behavior of the random fiber laser gradually stabilizes, leading to an improvement in spectral purity and the disappearance of higher-order Raman spectrum. With further increase in pump power, the pump light energy swiftly converts into signal light. Once the signal light intensity in the fiber reaches the threshold for second-order Raman scattering, the signal power starts transferring to a higher-order Raman frequency shift, resulting in a rapid amplification of the second-order Raman spectrum. Figure 6(b) illustrates the referenced normalized standard deviation (NSTD) of the output intensity. This NSTD decreases as the power is scaled up to higher levels, indicating a progressive improvement in the temporal stability of the signal laser. Although there have been reports discussing the temporal fluctuations[42], the precise dynamics underlying these processes remains somewhat unclear and necessitates further analysis by researchers.

The dynamics of intensity fluctuation transfer is an area of research that has seen progress in RRFLs. Understanding and controlling the intensity fluctuations in RRFLs is crucial for optimizing their performance and stability. Researchers have studied and developed techniques to manage and mitigate intensity fluctuations, thereby improving the performance and reliability of lasers. Furthermore, the RDFB mechanism introduces mode-free characteristics and distinctive statistical properties, making RRFLs fascinating and excellent platforms for scientific research and practical applications[31]. In an RRFL, it is important to note that multiple longitudinal modes can be generated and compete for gain within the laser cavity. This mode competition gives rise to irregular intensity fluctuations and rapid variations in output power over time.

4. Conclusion

In conclusion, we demonstrate an all-fiberized, purely passive SW RRFL directly pumped by multimode LDs. The power record of the purely passive RRFL excluding any active dopant in the whole system is obtained as 656 W at 1018 nm. To the best of our knowledge, this achievement also represents the highest power record of an RRFL utilizing multimode LDs for direct pumping at the wavelength. The slope efficiency is 94% and EO conversion efficiency is approximately 20%. The beam quality M^2 factor is 2.9 (which is ~20 times that of the pump) at the maximum output signal power, achieving the highest BE of 14.9 in RRFLs. The work could not only pave the way for achieving high-power SWs laser output through multimode LD direct pumping of passive fibers, but also provide a new insight into the realization of high-power, high-brightness RRFLs below 1 μm.

Acknowledgements

This work was supported by the National Natural Science Foundation of China (Nos. 62061136013 and 12174445). The authors thank Prof. Zilun Chen for providing the fiber end cap; and Mr. Liang Xiao for technical supporting in the experiment.

References

1. L. G. Wright, F. O. Wu, D. N. Christodoulides, and F. W. Wise, Nat. Phys. **18**, 1018 (2022).
2. P. Zhou, H. Xiao, J. Leng, J. Xu, Z. Chen, H. Zhang, and Z. Liu, J. Opt. Soc. Am. B **34**, A29 (2017).
3. M. N. Zervas and C. A. Codemard, IEEE J. Sel. Top. Quant. Electron. **20**, 219 (2014).
4. M. Jiang, H. Wu, Y. An, T. Hou, Q. Chang, L. Huang, J. Li, R. Su, and P. Zhou, PhotoniX **3**, 16 (2022).
5. C. Jauregui, C. Stihler, and J. Limpert, Adv. Opt. Photonics **12**, 429 (2020).
6. L. Dong, IEEE J. Quant. Electron. **59**, 6800108 (2023).
7. S. Naderi, I. Dajani, J. Grosek, and T. Madden, Opt. Express **24**, 16550 (2016).
8. J. Ye, J. Xu, J. Song, Y. Zhang, H. Zhang, H. Xiao, J. Leng, and P. Zhou, Photon. Res. **7**, 977 (2019).
9. Q. Chu, P. Zhao, H. Lin, Y. Liu, C. Li, B. Wang, C. Guo, X. Tang, C. Tang, and F. Jing, Appl. Opt. **57**, 2992 (2018).
10. B. Cao, C. Gao, Y. Ding, X. Xiao, C. Yang, and C. Bao, Opt. Lett. **47**, 4584 (2022).
11. P. Ju, W. Fan, B. Zhao, W. Gao, T. Zhang, G. Li, Q. Gao, and Z. Li, Infrared Phys. Technol. **111**, 103530 (2020).
12. C. Fan, Y. Chen, T. Yao, H. Xiao, J. Xu, J. Leng, P. Zhou, A. A. Wolf, I. N. Nemov, A. G. Kuznetsov, S. I. Kablukov, and S. A. Babin, Opt. Express **29**, 19441 (2021).
13. C. Fan, Y. An, Y. Li, X. Hao, T. Yao, H. Xiao, L. Huang, J. Xu, J. Leng, and P. Zhou, J. Lightwave Technol. **40**, 19 (2022).
14. S. A. Babin, High Power Laser Sci. Eng. **7**, e15 (2019).
15. R. Li, H. Li, H. Wu, H. Xiao, J. Leng, L. Huang, Z. Pan, and P. Zhou, Opt. Express **31**, 24423 (2023).
16. Z. Xie, Q. Fang, Y. Xu, X. Cui, Q. Sheng, W. Shi, and J. Yao, Opt. Eng. **58**, 106106 (2019).
17. G. Palma-Vega, T. Walbaum, M. Heinzig, S. Kuhn, C. Hupel, S. Hein, G. Feldkamp, B. Sattler, J. Nold, N. Haarlammert, T. Schreiber, R. Eberhardt, and A. Tuennermann, Opt. Lett. **44**, 2502 (2019).
18. C. Ottenhues, T. Theeg, K. Hausmann, M. Wysmolek, H. Sayinc, J. Neumann, and D. Kracht, Opt. Lett. **40**, 4851 (2015).
19. K.-J. Lim, S. K.-W. Seah, J. Y. Ye, W. W. Lim, C.-P. Seah, Y.-B. Tan, S. Tan, H. Lim, R. Sidharthan, A. R. Prasadh, C.-J. Chang, S. Yoo, and S.-L. Chua, Photon. Res. **8**, 1599 (2020).
20. Y. Glick, Y. Sintov, R. Zuitlin, S. Pearl, Y. Shamir, R. Feldman, Z. Horvitz, and N. Shafir, J. Opt. Soc. Am. B **33**, 1392 (2016).
21. J. Wang, G. Chen, L. Zhang, J. Hu, J. Li, B. He, J. Chen, X. Gu, J. Zhou, and Y. Feng, Appl. Opt. **51**, 7130 (2012).
22. C. P. Seah, T. Y. Ng, and S.-L. Chua, in *Advanced Solid State Lasers Conference* (2015), paper ATu2A.33.
23. P. Yan, X. Wang, Z. Wang, Y. Huang, D. Li, Q. Xiao, and M. Gong, IEEE J. Sel. Top. Quantum Electron. **24**, 0902506 (2018).
24. S. K. Kalyoncu and A. Yeniay, Appl. Opt. **59**, 4763 (2020).
25. N. Platonov, O. Shkurikhin, V. Fomin, D. Myasnikov, R. Yagodkin, A. Ferin, A. Doronkin, I. Ulyanov, and V. Gapontsev, Proc. SPIE **11260**, 1126003 (2020).

https://doi.org/10.1017/hpl.2024.8 Published online by Cambridge University Press

26. P. Wang, J. K. Sahu, and W. A. Clarkson, Opt. Lett. **31**, 3116 (2006).
27. J. Xu, J. Ye, W. Liu, J. Wu, H. Zhang, J. Leng, and P. Zhou, Photon. Res. **5**, 598 (2017).
28. J. Knall, M. Engholm, T. Boilard, M. Bernier, P.-B. Vigneron, N. Yu, P. D. Dragic, J. Ballato, and M. J. F. Digonnet, Optica **8**, 830 (2021).
29. N. Yu, M. Cavillon, C. Kucera, T. W. Hawkins, J. Ballato, and P. Dragic, Opt. Lett. **43**, 3096 (2018).
30. S. K. Turitsyn, S. A. Babin, A. E. El-Taher, P. Harper, D. V. Churkin, S. I. Kablukov, J. D. Ania-Castañón, V. Karalekas, and E. V. Podivilov, Nat. Photonics **4**, 231 (2010).
31. S. K. Turitsyn, S. A. Babin, D. V. Churkina, I. D. Vatnik, M. Nikulin, and E. V. Podivilov, Phys. Rep. **542**, 133 (2014).
32. J. Ye, X. Ma, Y. Zhang, J. Xu, H. Zhang, T. Yao, J. Leng, and P. Zhou, Photon. Res. **10**, 619 (2022).
33. E. A. Evmenova, A. G. Kuznetsov, I. N. Nemov, A. A. Wolf, A. V. Dostovalov, S. I. Kablukov, and S. A. Babin, Sci. Rep. **8**, 17495 (2018).
34. R. Li, H. Wu, H. Xiao, J. Leng, and P. Zhou, Opt. Laser Technol. **153**, 108204 (2022).
35. H. Wu, R. Li, H. Xiao, J. Leng, and P. Zhou, Opt. Express **29**, 34880 (2021).
36. X. Ma, J. Xu, J. Ye, Y. Zhang, L. Huang, T. Yao, J. Leng, Z. Pan, and P. Zhou, High Power Laser Sci. Eng. **10**, e5 (2022).
37. E. A. Zlobina, S. I. Kablukov, A. A. Wolf, A. V. Dostovalov, and S. A. Babin, Opt. Lett. **42**, 9 (2017).
38. Y. Glick, V. Fromzel, J. Zhang, N. Ter-Gabrielyan, and M. Dubinskii, Appl. Opt. **56**, B97 (2017).
39. A. G. Kuznetsov, S. I. Kablukov, E. V. Podivilov, and S. A. Babin, OSA Continuum **4**, 1034 (2021).
40. S. Hong, Y. Feng, and J. Nilsson, IEEE Photonics Technol. Lett. **30**, 1625 (2018).
41. S. Hong, Y. Feng, and J. Nilsson, IEEE Photonics Technol. Lett. **31**, 1995 (2019).
42. J. Ye, X. Ma, Y. Zhang, J. Xu, H. Zhang, T. Yao, J. Leng, and P. Zhou, PhotoniX **2**, 15 (2021).
43. J. Xu, J. Wu, J. Ye, J. Song, B. Yao, H. Zhang, J. Leng, W. Zhang, P. Zhou, and Y. Rao, Photon. Res. **8**, 1 (2020).
44. Y. Chen, T. Yao, H. Xiao, J. Leng, and P. Zhou, IEEE Photonics J. **12**, 1504713 (2020).
45. Y. Chen, T. Yao, H. Xiao, J. Leng, and P. Zhou, High Power Laser Sci. Eng. **8**, e33 (2020).
46. O. S. Sidelnikov, E. V. Podivilov, M. P. Fedoruk, A. G. Kuznetsov, S. Wabnitz, and S. A. Babin, Opt. Express **30**, 8212 (2022).
47. Y. Chen, T. Yao, H. Xiao, J. Leng, and P. Zhou, J. Lightwave Technol. **39**, 1785 (2021).
48. V. R. Supradeepa, F. Yan, and J. W. Nicholson, J. Opt. **19**, 023001 (2017).
49. G. P. Agrawal, J. Opt. Soc. Am. B **40**, 715 (2023).
50. S. A. Babin, E. I. Dontsova, and S. I. Kablukov, Opt. Lett. **38**, 3301 (2013).

https://doi.org/10.1017/hpl.2024.8 Published online by Cambridge University Press